Double tearing mode in plasmas with anomalous electron viscosity

J. Q. Dong

Southwestern Institute of Physics, P.O. Box 432, Chengdu, China

S. M. Mahajan and W. Horton

Institute for Fusion Studies, The University of Texas at Austin, Austin, USA

(Dated: February 24, 2003)

The linear behavior of the double tearing mode in plasmas with a phenomenological anomalous electron viscosity is investigated within the framework of magnetohydrodynamic (MHD) theory. In the large Reynolds number $R = \tau_v/\tau_h$ (τ_v and τ_h are, respectively, the viscosity penetration time of the magnetic field and the Alfvén time for a plasma sheet of width a) limit, the growth rate is found to scale as $R^{-1/5}$ if the two resonant surfaces, at $x = \pm x_s$, are close enough to satisfy $x_s/a \ll (k_y a)^{-11/15} R^{-1/15}$. For larger separation between the resonant surfaces, the growth rate transits to a $R^{-1/3}$ scaling. The transition occurs at $x_s/a \sim (k_y a)^{-11/15} R^{-1/15}$. The $R^{-1/5}$ is shown to be closely correlated with the violation of the constant-ψ approximation. The nonlinear velocity perturbations associated with the unstable double tearing mode are estimated to saturate at a level high enough to serve as a trigger for the formation of transport barriers observed in advanced tokamaks.

I. INTRODUCTION

One of the characteristics for an advanced tokamak (AT) operation is a non-monotonic safety factor q profile, providing a region with negative magnetic shear.[1,2] Such a configuration is prone to the excitation of a double tearing mode (DTM), an instability peculiar to a plasma with multiple resonant surfaces ($\boldsymbol{k} \cdot \boldsymbol{B} = 0$). With magnetic islands on sufficiently close adjacent resonant surfaces interacting and effectively enhancing each other, the double tearing mode turns out to be a much stronger instability than the standard (i.e., constant-ψ) tearing mode.

On the other hand the AT mode of operation is considered to be highly desirable because of the realization of high performance regimes in which the so-called internal transport barriers (ITBs) are formed with the simultaneous appearance of highly sheared localized poloidal flows. In this paper we will attempt to show a possible causal relationship between the DTM and the experimentally observed shear flows.

The double tearing mode, driven by plasma resistivity, has been studied by several authors.[3–10] The linear growth rate of the mode goes as $S^{-1/3}$ when the separation of the resonant surfaces ($x = \pm x_s$) is sufficiently small, i.e. x_s satisfies the inequality

$$\frac{x_s}{a} < (k_y a)^{-7/9} S^{-1/9}. \tag{1}$$

When the separation of the resonant surfaces is large, i.e., the inequality in Eq. (1) is reversed, the islands do not interact strongly, and the growth rate of the double tearing mode scales as $S^{-3/5}$ as it is for the standard tearing mode.[3] Here, $S = \tau_r/\tau_h$ is the magnetic Reynolds number with $\tau_r = 4\pi a^2/c^2\eta$ and $\tau_h = a/v_A$ being the resistive diffusion time and the poloidal Alfvén time of a plasma column of scale width a, respectively; c is the speed of light, η is the plasma resistivity, v_A is the poloidal Alfvén velocity. The island growth of the double tearing mode in early nonlinear stage is analyzed by Yu.[10]

In contrast to extensive studies on tearing modes driven by plasma resistivity, investigations on tearing modes driven by plasma viscosity are rather scant. Experiments indicate, however, that anomalous viscosity may be present in tokamak plasmas due to electromagnetic turbulence.[11,12] Bootstrap drive of neoclassical tearing modes in the presence of anomalous viscosity is performed recently by Konovalov *et al.*[13] Tearing modes driven by anomalous electron viscosity due to braiding magnetic field lines have been considered as

possible candidates responsible for disruptive instability.[14,15] It is found that the growth rates of $m \geq 2$ and $m = 1$ electron viscosity tearing modes scale as $\gamma \sim R^{-1/3}$ and $\gamma \sim R^{-1/5}$, respectively. Here, $R = \tau_v/\tau_h$ is the fluid dynamic Reynolds number, while $\tau_v = 4\pi a^4 n_e e^2/c^2\mu_e m_e = \omega_{pe}^2 a^4/c^2\mu_e$ is the viscosity diffusion time of plasma current over a sheet of width a, μ_e is the electron viscosity diffusion coefficient. In strong electromagnetic drift-wave turbulence the coefficient μ_e may be comparable to the electron thermal diffusivity which can be a few m^2/s. The electron viscosity tearing mode was, later, studied by Aydemir as a possible candidate for experimentally observed fast sawtooth crashes.[16] It was found that the electron viscosity driven modes had higher growth rates than the corresponding resistivity driven modes in present fusion devices if the electron viscosity had a value comparable to that of the anomalous electron thermal diffusivity. The viscosity considered here is expected to contribute to the parallel electron motion equation and to cause plasma current penetration across equilibrium magnetic flux surfaces.

The subject of this paper is a detailed linear analysis of the double tearing mode driven by anomalous electron viscosity. In Sec. II, the governing MHD equations including resistivity and viscosity are presented, and an approximate analytic dispersion relation for the double tearing mode (following the methods of Ref. 3) is derived and discussed in Sec. III. In Sec. IV we turn to a well developed computer code to study the instability in detail; the eigenvalues and the structure of the eigenfunctions for a variety of parameters are obtained. Emphasis is placed on the detailed analysis of the perturbed poloidal velocity profiles. The conclusions and discussion are presented in Sec. V. The possible correlation of the nonlinear DTM driven by electron viscosity with the dynamics of ITB formation is also emphasized.

II. EQUILIBRIUM AND MHD EQUATIONS

We consider the standard sheared slab configuration,

$$\boldsymbol{B}_0(x) = B_{0y}(x)\widehat{\boldsymbol{y}} + B_{0z}(x)\widehat{\boldsymbol{z}}, \tag{2}$$

where $B_{0y}(x)$ equals zero at $x = \pm x_s$. The plasma sheet is of length a in the x-direction, has a current in the z-direction, and its equilibrium flow velocity $\boldsymbol{V}_0 = 0$. The stability of this initial configuration will be examined with respect to two-dimensional, incompressible perturbations. For this restricted class of perturbations, the vector fields are expressible

in terms of the two scalar potentials: the flux function $\psi(x, y, t)$, and the stream function $\phi(x, y, t)$,

$$\boldsymbol{B}_\perp = \nabla\psi \times \hat{\boldsymbol{z}}, \tag{3}$$

and

$$\boldsymbol{V}_\perp = \nabla\phi \times \hat{\boldsymbol{z}}. \tag{4}$$

With electron viscosity, the Ohm's law becomes

$$\boldsymbol{E} = \eta\boldsymbol{j} - \frac{1}{c}\boldsymbol{V} \times \boldsymbol{B} - \frac{m_e\mu_e}{n_e e^2}\nabla^2\boldsymbol{j}. \tag{5}$$

It is straightforward to write the z-component of the curl of Eq. (5) as

$$\frac{\partial\psi}{\partial t} = -\boldsymbol{V}\cdot\nabla\psi + \frac{c^2}{4\pi}\eta\nabla^2\psi - \frac{m_e\mu_e c^2}{4\pi n_e e^2}\nabla^4\psi, \tag{6}$$

after using Eq. (3) and Faraday's law. The z-component of plasma motion equation may be written as

$$\frac{\partial}{\partial t}(\nabla^2\phi) = -(\boldsymbol{V}\cdot\nabla)\nabla^2\phi + \frac{1}{4\pi\rho}[\nabla(\nabla^2\psi)\times\nabla\psi]\cdot\hat{\boldsymbol{z}}, \tag{7}$$

where ρ is the mass density of the plasma. The close set of Eqs. (6) and (7) is our starting point for the stability analysis. Assuming all perturbations in the form $f \sim f(x)\exp(ik_y y + \gamma t)$, we get the linearized version of Eqs. (6) and (7):

$$\gamma\psi_1 = V_x B_{0y}(x) + \frac{\eta c^2}{4\pi}\left(\frac{\partial^2\psi_1}{\partial x^2} - k_y^2\psi_1\right) - \frac{\mu_e c^2}{\omega_{pe}^2}\left(\frac{\partial^4\psi_1}{\partial x^4} + k_y^4\psi_1\right), \tag{8}$$

and

$$\rho\gamma\left(\frac{\partial^2\phi}{\partial x^2} - k_y^2\phi\right) = -\frac{i}{4\pi}k_y B_{0y}''(x)\psi_1 + \frac{ik_y}{4\pi}B_{0y}(x)\left(\frac{\partial^2\psi_1}{\partial x^2} - k_y^2\psi_1\right), \tag{9}$$

where η, ρ and μ_e have been taken as constants and the double prime denotes second derivative with respect to x.

Normalizing all lengths to a, time to τ_h, and the magnetic field to some standard measure B_0, Eqs. (8) and (9) convert to the following dimensionless from,

$$\gamma\tau_h\psi_1 = \gamma\tau_h\xi B_{0y}(x) + \frac{1}{S}\left(\frac{\partial^2\psi_1}{\partial x^2} - \alpha^2\psi_1\right) - \frac{1}{R}\left(\frac{\partial^4\psi_1}{\partial x^4} + \alpha^4\psi_1\right), \tag{10}$$

and

$$(\gamma\tau_h)^2\left(\frac{\partial^2\xi}{\partial x^2} - \alpha^2\xi\right) = \alpha^2 B_{0y}''(x)\psi_1 - \alpha^2 B_{0y}(x)\left(\frac{\partial^2\psi_1}{\partial x^2} - \alpha^2\psi_1\right), \tag{11}$$

where $\alpha = k_y a$, $\xi = ik_y\phi/\gamma a$, $S = \tau_r/\tau_h$, $R = \tau_v/\tau_h$. It is easy to note from Eq. (6) that $\tau_v = a^4\omega_{pe}^2/\mu_e c^2$ is the viscosity diffusion time for a magnetic field over a plasma sheet of width a.

III. TWO-SPACE-SCALE ANALYSIS AND DISPERSION RELATION

Equation (10) indicates that the dissipation terms (the second and third terms on the right-hand side) are important only in a narrow layer around $x = \pm x_s$ where the magnetic field B_{y0} equals zero. In the regions between the rational surfaces ($|x| < x_s$) and outside the two surfaces ($|x| > x_s$), the effects of the dissipation terms are negligible. Therefore, we adapt the two-space-scale analysis usually used for the resistive tearing mode studies. We employ ideal magnetohydrodynamics in the outer regions, i.e., the equations obtained when $S \to \infty$ and $R \to \infty$ in Eq. (10). The solutions obtained in these two regions (exterior solutions) must join smoothly with the dissipative (interior) solutions obtained from Eq. (10) and valid near each resonant surface.

We first solve the ideal MHD. Substituting

$$\psi_1(x) = B_{0y}(x)\xi(x), \tag{12}$$

a consequence of Eq. (10), into Eq. (11), we find

$$\frac{d}{dx}\left\{\left[(\gamma\tau_h)^2 + (\alpha B_{0y}(x))^2\right]\frac{d\xi}{dx}\right\} = \alpha^2\left[(\alpha B_{0y}(x))^2 + (\gamma\tau_h)^2\right]\xi. \tag{13}$$

This equation governs the behavior of the double kink mode in a slab. The inertial terms $(\gamma\tau_h)$ are negligible in comparison with the αB_{0y} terms in the ideal MHD regions and Eq. (13) reduces to,

$$\frac{d}{dx}\left[(\alpha B_{0y}(x))^2\right]\frac{d\xi}{dx} = \alpha^4 B_{0y}^2(x)\xi, \tag{14}$$

which may be solved in terms of a power series expansion in the small parameter $\alpha^2 x_s^2$:

$$\xi = \xi_0 + \xi_1 + \dots \ .$$

To the lowest order, Eq. (14) reduces to

$$\frac{d}{dx}\left[(\alpha B_{0y}(x))^2\right]\frac{d\xi_0}{dx} = 0. \tag{15}$$

Because the displacement ξ_0 is symmetric about the $x = 0$ surface, and $|x| = x_s$ are the singularity surfaces, the solution for Eq. (15) may be written as[17]

$$\xi_0(x) = \xi_\infty = \begin{cases} \text{const}, & |x| < x_s; \\ 0, & |x| > x_s. \end{cases} \tag{16}$$

The first order solution is given by

$$\frac{1}{\xi_\infty}\frac{d\xi_1}{dx} = \begin{cases} \left(\dfrac{\alpha}{B_{0y}(x)}\right)^2 \displaystyle\int_0^x B_{0y}^2(x')dx', & |x| < x_s, \\ \left(\dfrac{\alpha}{B_{0y}(x)}\right)^2 \displaystyle\int_0^{x_s} B_{0y}^2(x')dx', & |x| > x_s. \end{cases} \tag{17}$$

Near $x = x_s$, we expand $B_{0y}(x)$ as a Taylor series and neglect the two terms on the right-hand side of Eq. (13). Then, the solution that matches Eq. (16) is

$$\xi = \frac{1}{2}\xi_\infty \left\{1 - \frac{1}{\pi}\arctan\left[\alpha B'_{0y}(x - x_s)/\gamma\tau_h\right]\right\}, \tag{18}$$

where $B'_{0y} = B'_{0y}(x_s)$.

The growth rate of the double kink mode, now, is found by equating $d\xi/dx$ obtained from Eq. (18) in the limit $\alpha B'_{0y}(x - x_s)/\gamma\tau_h \to -\infty$ with $d\xi_1/dx$ obtained from Eq. (17) in the limit $x \to x_s^-$,

$$\gamma_h\tau_h = -\frac{\pi\alpha^3}{B'_{0y}}\int_0^{x_s} B_{0y}^2(x')dx'. \tag{19}$$

Thus we find from Eq. (19) that with pure MHD driving energy alone, the double kink mode is stable in slab geometry approaching marginal stability in the limit $\alpha x_s \to 0$.[3]

Dissipation (resistivity and viscosity), however, may provide a mechanism for the marginally stable double tearing mode to go unstable. Even with dissipation, the outer region (away from the resonant surfaces $x = \pm x_s$) solutions, Eqs. (16) and (17), remain unchanged while the inner region is now described by Eqs. (10) and (11)

$$(\gamma\tau_h)^2\xi'' = -\alpha^2 B'_{0y}(x - x_s)\psi_1'', \tag{20}$$

$$\gamma\tau_h\psi_1 = \gamma\tau_h B'_{0y}(x - x_s)\xi + \frac{1}{S}\frac{\partial^2\psi_1}{\partial x^2} - \frac{1}{R}\frac{\partial^4\psi_1}{\partial x^4}, \tag{21}$$

where the double prime denotes second derivative with respect to x, and α^2 has been neglected in comparison with d^2/dx^2.

Under the transformations $x - x_s \to x$, $\psi_1/B'_{0y} \to \psi_1$, $\xi \to -\xi$, Eqs. (20) and (21) become

$$\xi'' = \frac{x}{\lambda^2}\psi_1'', \tag{22}$$

$$\psi_1 = -x\xi + \frac{\varepsilon}{\lambda}\psi_1'' - \frac{\sigma}{\lambda}\psi_1^{(4)}, \tag{23}$$

where $\lambda = \gamma\tau_h/\alpha B'_{0y}$, $\varepsilon = 1/S\alpha B'_{oy}$, $\sigma = 1/R\alpha B'_{0y}$.

These inner region equations have to be solved with the boundary condition that the solution matches the ideal MHD solution as $|x| \to \infty$. Equations (22) and (23) may be converted into a single sixth order differential equation for ξ,

$$-\lambda\sigma\left[\frac{24}{x^5}\xi'' - \frac{24}{x^4}\xi^{(3)} + \frac{12}{x^3}\xi^{(4)} - \frac{4}{x^2}\xi^{(5)} + \frac{1}{x}\xi^{(6)}\right]$$

$$+\lambda\varepsilon\left[\frac{2}{x^3}\xi'' - \frac{2}{x^2}\xi^{(3)} + \frac{1}{x}\xi^{(4)}\right] - 2\xi' - \left(x + \frac{\lambda^2}{x}\right)\xi'' = 0, \tag{24}$$

where $\xi^{(n)}$ indicates the nth derivative with respect to x. This equation has six independent solutions. It is not difficult to see that the asymptotic form of one of these solutions, $\xi = \text{const}/x$ with $d\xi/dx = \text{const}/x^2$, matches the outer solution perfectly. Let us write this solution as

$$\xi = \frac{1}{2}\xi_\infty + \xi_{\text{odd}}(x), \tag{25}$$

and the outer solution, Eq. (17), as

$$\frac{1}{\xi_\infty}\frac{d\xi}{dx} = -\frac{\lambda_h}{\pi}\frac{1}{x^2}, \tag{26}$$

where

$$\lambda_h = -\frac{\pi\alpha^2}{B_{0y}'^2}\int_0^{x_s} B_{0y}'^2(x')dx', \tag{27}$$

and $\xi_{\text{odd}}(x)$ in Eq. (25) has to satisfy the boundary condition

$$\frac{x^2}{2}\frac{d}{dx}(\ln\xi_{\text{odd}}) = \begin{cases} -\frac{1}{\pi}\lambda_h, & \text{for} \quad x \to -\infty: \\ \frac{1}{\pi}\lambda_h, & \text{for} \quad x \to \infty \end{cases} \tag{28}$$

since ξ_{odd} is an odd function of x.

For a given λ_h, σ and ε (representing viscosity and resistivity) Eqs. (22) and (23) may be solved numerically (with appropriate conditions for $\xi_{\text{odd}}(0) = 0$ and ψ_1) to determine the dependence of the effective eigenvalue λ on λ_h, i.e, the dispersion relation of the mode. The present work, however, is limited to the double tearing mode driven by electron viscosity. Approximate analytical work is presented below.

If resitivity is neglected ($\varepsilon = 0$) Eqs. (22) and (23) reduce to

$$\xi'' = \frac{x}{\lambda^2}\psi_1'', \tag{29}$$

$$\psi_1 = -x\xi - \frac{\sigma}{\lambda}\psi_1^{(4)}. \tag{30}$$

Following Ref. 17, we introduce the function

$$\chi(x) = x\psi_1' - \psi_1 = \lambda^2 \frac{d\xi}{dx} + \chi_\infty, \tag{31}$$

in terms of which, Eqs. (29) and (30) may be combined into one equation,

$$\sigma\lambda \left[\frac{d^4\chi}{dx^4} - \frac{4}{x}\frac{d^3\chi}{dx^3} + \frac{8}{x^2}\frac{d^2\chi}{dx^2} - \frac{8}{x^3}\frac{d\chi}{dx} \right] + (\lambda^2 + x^2)\chi = x^2\chi_\infty, \tag{32}$$

where the constant χ_∞ is to be determined from the asymptotic behavior of the solution.

Manipulating Eq. (30), we derive

$$\xi = -\frac{\psi_1}{x} - \frac{\sigma}{\lambda x}\frac{d^4\psi}{dx^4} = -\frac{1}{x}\chi(x) + \int_x^\infty \frac{1}{x'}\frac{d\chi}{dx'}dx' - \frac{\sigma}{\lambda x}\left[\frac{2}{x^3}\frac{d\chi}{dx} - \frac{2}{x^2}\frac{d^2\chi}{dx^2} + \frac{1}{x}\frac{d^3\chi}{dx^3} \right], \tag{33}$$

and

$$\xi_\infty \simeq \int_{-\infty}^\infty \frac{1}{x}\frac{d\chi}{dx}dx \simeq 2\int_0^\infty \frac{1}{x}\frac{d\chi}{dx}dx, \tag{34}$$

since $\xi \to \xi_\infty$ when $x \to -\infty$. In addition, we know that $d\xi/dx \to \text{const}/x^2$ when $x \to -\infty$. Defining

$$\frac{d\xi}{dx}\,|_{x\to-\infty} = \frac{\chi_\infty}{x^2}, \tag{35}$$

and comparing it with Eq. (28), we deduce

$$\chi_\infty = \frac{1}{\pi}\lambda_h\xi_\infty \simeq \frac{2\lambda_h}{\pi}\int_0^\infty \frac{d\chi}{dx}\frac{dx}{x}. \tag{36}$$

Equation (36) may be considered as the boundary condition for the solution of Eq. (32).

To obtain approximate solution for Eq. (32), we notice that in the ideal MHD limit, $\sigma \to 0$, Eq. (32) yields

$$\chi = \frac{x^2}{\lambda^2 + x^2}\chi_\infty. \tag{37}$$

Substituting this solution into the boundary condition, Eq. (36), we may easily show that

$$\lambda = \lambda_h,$$

i.e., the perturbation is an ideal MHD mode as it was supposed to be.

When the ideal MHD mode is marginally stable, $\lambda_h = 0$, $\chi_\infty = 0$ and Eq. (32) becomes

$$\sigma\lambda \left[\frac{d^4\chi}{dx^4} - \frac{4}{x}\frac{d^3\chi}{dx^3} + \frac{8}{x^2}\frac{d^2\chi}{dx^2} - \frac{8}{x^3}\frac{d\chi}{dx} \right] + (\lambda^2 + x^2)\chi = 0. \tag{38}$$

To order x^3, Eq. (38) allows the solution

$$\chi = A\exp\left[-x^2/2^{6/5}\sigma^{2/5}\right], \qquad \lambda = \sigma^{1/5}/2^{2/5}, \tag{39}$$

where the constant coefficient A is easily obtained from the boundary condition, Eq. (36); the final solution is

$$\chi = \frac{\xi_\infty \sigma^{1/5}}{\sqrt{\pi} 2^{2/5}} \exp\left[-x^2/2^{6/5}\sigma^{2/5}\right]. \tag{40}$$

Equation (30) tells us that in the case of ideal MHD marginal stability, the growth rate of the tearing mode driven by electron viscosity is

$$\gamma = \frac{(\alpha B'_{0y})^{4/5}}{2^{2/5}\tau_h^{4/5}\tau_v^{1/5}}. \tag{41}$$

It is the same as that for the $m = 1$ tearing mode driven by electron viscosity.[14]

Now, we look for a more general solution of Eq. (32). Introducing $\zeta = x^2/\lambda^{1/3}\sigma^{1/3}$, $\widehat{\lambda} = \lambda/\sigma^{1/5}$, we transfer Eq. (32) into

$$\zeta^2 \frac{d^4\chi}{d\zeta^4} + \zeta \frac{d^3\chi}{d\zeta^3} - \frac{1}{4}\frac{d^2\chi}{d\zeta^2} + \frac{1}{16}(\widehat{\lambda}^{5/3} + \zeta)\chi = \zeta\chi_\infty. \tag{42}$$

We look for an approximate solution for this equation in the following. First, in comparison with Eq. (39), we neglect the term with ζ^2. Then, we assume that the equation has a solution of the form

$$\chi = A\left\{1 + B\int_0^1 t^l(1+t)^m \exp\left[-\frac{\zeta}{\alpha'}\left(\frac{1-t}{1+t}\right)\right] dt\right\}, \tag{43}$$

where the constants $A,\ B,\ l,\ m,$ and α' are readily determined (by direct substitution) to be

$$A = \chi_\infty, \quad B = -\frac{\widehat{\lambda}^{5/3}}{2^{m+1}\alpha'}, \quad l = \frac{\widehat{\lambda}^{5/3}}{3\alpha'} - \frac{13}{12}, \quad m = \frac{\widehat{\lambda}^{5/3}}{3\alpha'} + \frac{5}{4}, \quad \alpha' = 2^{4/3}. \tag{44}$$

Invoking Eq. (36), we derive the dispersion relation,

$$\lambda = \lambda_h \left\{ \frac{\widehat{\lambda}^{5/2}}{16 \cdot 2^{\left(\frac{\widehat{\lambda}^{5/3}}{3\alpha'} + \frac{1}{4}\right)}} \cdot \frac{\Gamma\left(\frac{\widehat{\lambda}^{5/3}}{6\sqrt[3]{2}} - \frac{1}{12}\right)}{\Gamma\left(\frac{\widehat{\lambda}^{5/3}}{6\sqrt[3]{2}} + \frac{17}{12}\right)} \cdot F\left(-\frac{\widehat{\lambda}^{5/3}}{6\sqrt[3]{2}} - \frac{3}{4}, \frac{\widehat{\lambda}^{5/3}}{6\sqrt[3]{2}} - \frac{1}{12}, \frac{\widehat{\lambda}^{5/3}}{6\sqrt[3]{2}} + \frac{17}{12}, -1\right) \right\}, \tag{45}$$

where F is the hypergeometric function,[18]

$$F(a,b,c,z) = \frac{\Gamma(c)}{\Gamma(a)\Gamma(b)} \sum_{n=0}^{\infty} \frac{\Gamma(a+n)\Gamma(b+n)}{\Gamma(c+n)} \frac{z^n}{n!}. \tag{46}$$

It is easy to verify that the function F in Eq. (46) converges absolutely. The numerical solution of the dispersion relation, Eq. (45), is displayed as a plot of $\widehat{\lambda}$ versus $\widehat{\lambda}_h$ in Fig. 1. The approximate analytical results are in very good agreement with the numerical results

obtained for the $m = 1$ mode when $\widehat{\lambda}$ is not too large.[14] The general behavior tends to be similar though one notices clear differences for large $\widehat{\lambda}$. Small $\widehat{\lambda}$ corresponds to $\widehat{\lambda}_h \lesssim 0$, i.e., the ideal MHD double kink mode is stable or marginally stable. It is precisely in these two cases that the study of the double tearing mode driven by electron viscosity is important; the approximate analytic solution given above is, therefore, appropriate for the study of the electron viscosity double tearing mode.

The dispersion relation, Eq. (45), may be further approximated as

$$\lambda = \lambda_h \left\{ \frac{\widehat{\lambda}^{5/2}}{16 \cdot \sqrt[4]{2}\left(1 + \frac{\widehat{\lambda}^{5/3}}{6\sqrt[3]{2}} \ln 2\right)} \left[1 + \frac{\left(\frac{\widehat{\lambda}^{5/3}}{6\sqrt[3]{2}} + \frac{3}{4}\right)\left(\frac{\widehat{\lambda}^{5/3}}{6\sqrt[3]{2}} - \frac{1}{12}\right)}{\frac{\widehat{\lambda}^{5/3}}{6\sqrt[3]{2}} + \frac{17}{12}} \right] \times \frac{\Gamma\left(\frac{\widehat{\lambda}^{5/3}}{6\sqrt[3]{2}} - \frac{1}{12}\right)}{\Gamma\left(\frac{\widehat{\lambda}^{5/3}}{6\sqrt[3]{2}} + \frac{17}{12}\right)} \right\}. \tag{47}$$

Two special limits are easy to understand:

1) if $\lambda_h = 0$ then $\widehat{\lambda} = 1/2^{2/5}$, i.e.,

$$\lambda = \sigma^{1/5}/2^{2/5},$$

which is exactly the same as Eq. (39);

2) if $\widehat{\lambda}_h < 0$ and $|\widehat{\lambda}_h| \gg 1$, then $\widehat{\lambda} \ll 1$ according to Fig. 1 and we have from Eq. (47) that

$$\lambda = \text{const}\frac{\sigma^{1/3}}{\lambda_h^{2/3}}. \tag{48}$$

Now, we discuss the requirements that will let the viscosity- driven double tearing mode to have a growth rate given in Eq. (39), and then to transit to that given by Eq. (48). On double differentiation with respect to x, Eq. (29) becomes

$$\xi^{(4)} = \frac{x}{\lambda^2}\psi_1^{(4)} + \frac{2}{\lambda^2}\psi_1^{(3)}.$$

Substituting $\psi_1^{(4)}$ from Eq. (30) into this equation gives us

$$\xi^{(4)} = \frac{x}{\lambda\sigma}[-\psi_1 + x\xi] + \frac{2}{\lambda^2}\psi^{(3)}.$$

Comparing the ξ terms in the equation, we get an estimate for the thickness of the dissipation layer:

$$\Delta \simeq (\lambda\sigma)^{1/6} \simeq \left[\gamma\tau_h/(\alpha B'_{0y})^2 R\right]^{1/6}. \tag{49}$$

It has to be pointed out that the dispersion relation given in Fig. 1 is valid only for $\Delta \ll x_s$; otherwise there are no separable inner and outer regions. it is also essential to remember that the solution in the outer region is valid only when $\alpha x_s < 1$.

Remembering

$$\widehat{\lambda} = \frac{\lambda}{\sigma^{1/5}} = \gamma\tau_h (R/\alpha^4 B_{0y}'^4)^{1/3}, \tag{50}$$

$$\widehat{\lambda}_h = \frac{\lambda_h}{\sigma^{1/5}} = \gamma_h\tau_h \left(R/\alpha^4 B_{0y}'^4\right)^{1/3}, \tag{51}$$

and the discussion following Eq. (18) (leading to $|\widehat{\lambda}_h| \ll 1$ for $\alpha x_s \ll 1$), we get

$$\widehat{\lambda} = \frac{1}{2^{2/5}},$$

and the growth rate

$$\gamma\tau_h \simeq 0.8 \left(\frac{\alpha^4 B_{0y}'^4}{R}\right)^{1/5}. \tag{52}$$

which scales as $R^{-1/5}$.

The conditions $|\widehat{\lambda}_h| \ll 1$ and $\Delta \ll x_s$ impose (assuming $B_{0y}' = 1$)

$$\left(\frac{\alpha}{R}\right)^{1/5} \ll \alpha x_s \ll \left(\frac{\alpha^4}{R}\right)^{1/15}. \tag{53}$$

If x_s is sufficiently large, then $|\widehat{\lambda}_h| \gg 1$ and $\widehat{\lambda} \ll 1$, and we have

$$\gamma\tau_h = \frac{\text{const.}}{(\gamma_h\tau_h)^{2/3}} \left(\frac{\alpha^4 B_{0y}'^4}{R}\right)^{1/3}. \tag{54}$$

with the growth rate scaling as $R^{-1/3}$.

The conditions $|\widehat{\lambda}_h| \gg 1$ and $\alpha x_s \ll 1$ imply

$$\left(\frac{\alpha^4}{R}\right)^{1/15} \ll \alpha x_s \ll 1. \tag{55}$$

Therefore, it is explicit that the transition from the $R^{-1/5}$ to $R^{-1/3}$ occurs roughly at $\alpha x_s \sim (\alpha^4/R)^{1/15}$.

The current penetration time due to viscosity over the tearing layer may be estimated as

$$\tau_\Delta \simeq \frac{\Delta^4 \omega_{pe}^2}{\mu_e c^2} = \Delta^4 \tau_h R, \tag{56}$$

where Δ is given by Eq. (49). This results in

$$\gamma\tau_\Delta = \gamma \left(\gamma\tau_h/\alpha^2 B_{0y}'^2 R\right)^{2/3} \tau_h R = \widehat{\lambda}^{5/3}. \tag{57}$$

If the ideal MHD mode is marginally stable, then $\widehat{\lambda} \simeq 1$ from Fig. 1. The current penetration time is comparable with the tearing mode growing time and the constant-ψ approximation is not valid. The mode grows according to Eq. (52). On the other hand, if the ideal MHD mode is stable, then $\widehat{\lambda} \ll 1$. The tearing mode growth time is much longer than the current penetration time. In this case, ψ_1 may approximately be considered as a constant over the tearing layer. The growth rate is give by Eq. (54) in this regime.

IV. NUMERICAL RESULTS

We employ the same configuration as used in Ref. 3

$$B_{0y}(x) = 1 - (1 + b_c)\mathrm{sech}(\zeta x), \tag{58}$$

where

$$\zeta x_s = \mathrm{sech}^{-1}\left[1/(1 + b_c)\right]. \tag{59}$$

Equation (58) has the properties that $B_{0y}(\pm x_s) = 0$, $B_{0y}(0) = -B_c$, and $B_{0y} \to 1$ as $x \to \pm\infty$. The constant B_c is chosen so as to make $B'_{0y}(x_s) = \pi/2$ (Ref. 3). We do not need to specify $B_{0z}(x)$ and $P_0(x)$ since incompressible equations are used. We assume that the resistive and the electron viscosity diffusion times are much longer than the double tearing mode growing time and the equilibrium is static. The resistivity and the viscosity are both assumed to be constant.

Equations (10) and (11) are solved as an eigenvalue problem using a shooting code. Only symmetric modes are considered for which $d\xi/dx|_{x=0} = d^3\psi/dx^3|_{x=0} = 0$ are the required boundary conditions. In addition, the normalization $\psi_1(0) = 1$ is applied. At the outer boundary $x = \pm x_w$, $\psi_1 = 10^{-5}$ and $\xi = d\xi/dx = 0$ are employed.

With the grid number fixed at 200, the results presented below were checked to be approximately independent of x_w. The growth rate changes less than 0.1% for a 50% change of x_w.

The code was benchmarked with the results on the resistive double tearing mode in Ref. 3 first by taking a sufficiently large R value such as 10^{10} for $S = 10^6$ and comparing numerical results with Fig. 5 of Ref. 3. Then the electron viscosity was introduced, and the related double tearing modes were studied by decreasing R and increasing S. Shown in Fig. 2 is the normalized growth rate $\gamma\tau_h$ as a function of the wave number α for $x_s = 0.25$ (a) and 0.7 (b). The lines, from the top to the bottom, correspond to $R = 10^5,\ 10^6,\ 10^7$, and 10^8 in Fig. 2(a), and to $R = 10^4,\ 10^5,\ 10^6,\ 10^7$, and 10^8in Fig. 2(b), respectively.The growth rate is checked to be independent of $S \sim 10^7$ in all the cases. The electron viscosity double tearing mode always dominates in the parameter regime studied here for $R \lesssim S$. The growth rate increases with α in both cases whereas it increases with α for $x_s = 0.25$ and has a maximum around $\alpha \sim 0.35$ for $x_s = 0.7$ in the resistive double tearing case.

Shown in Fig. 3 is the growth rate as a function of the fluid dynamic Reynolds number

R for $x_s = 0.25$ (the short line) and 0.7 (the longer line); the wavenumber is $\alpha = 0.75$. The mode growth rate follows the $R^{-1/3}$ scaling for $x_s = 0.25$ while there is a transition from $R^{-1/3}$ to $R^{-1/5}$ at $R \sim 10^6$ for $x_s = 0.7$. This is in agreement with the analytic results given in Sec. III.

The eigenfunctions $\psi_1(x)$, $\xi(x)$ and the perturbations of the parallel current density j_{iz} and the poloidal velocity V_y are given in Figs. 4, 5 and 6 for $x_s = 0.25$, 0.7 and 0.1, respectively. The other parameters for Fig. 4 (5) are $\alpha = 0.25(0.5)$, $S = 9.4 \times 10^5$ (10^8) and $R = 10^6$ (10^8). It is clearly shown that the changes of ψ_1 across the tearing layers are significant in Fig. 4(a); the constant-ψ approximation breaks down in this case. In addition, the perturbation of the parallel current density is spread over the entire region between the two rational surfaces, and peaks at the center [Fig. 4(b)]. On the other hand, the perturbation of the flux ψ_1 does not change much across the tearing layers in Fig.5(a); the constant-ψ approximation is valid in this case. In addition, the perturbation of the parallel current density sharply peaks at the two rational surfaces and is about one half the peak current density at the center [Fig. 5(b)]. Thus, the total integrated perturbed current across the layer is small compared to that of the current layers in the other cases. The parameters in Fig. 6 are $\alpha = 0.25$, $S = 10^8$ and $R = 10^4$. Here, besides the substantial changes in the perturbed flux ψ_1 and the displacement ξ at the rational surfaces like that in Fig. 4, the perturbed parallel current is much more peaked at the center. This is similar to the binary branch studied by Mahajan and Hazeltine for resistive tearing modes in configurations with a parabolic safety factor q.[4] The most notable characteristics of Fig. 6 in comparison with Fig. 5 is in the perturbed poloidal velocity profile. The V_y profile of Fig. 5 has two strong peaks highly localized at the two rational surfaces, and is essentially zero in the between region. On the other hand, the profile displayed in Fig. 6 is a rather broad distribution that is nonzero over the whole range between the two rational surfaces and extends far beyond. The V_y profile is a transition between counter flowing shear flows of Fig. 4 and the parallel flows of Fig. 5.

V. CONCLUSIONS AND DISCUSSION

Two distinct kinds of tearing modes driven by finite plasma resistivity in configurations with non-monotonic safety factor profile were identified and analyzes by Pritchett *et al.*,[3] and

by Mahajan and Hazeltine.[4] Two analogous kinds of tearing modes but driven by anomalous electron viscosity in the same equilibrium magnetic configuration,[3] are studied in this paper. One of the principal aims of this investigation is the search for an engine for the creation of transport barriers. It is found that the growth rates of the modes scale as $R^{-1/5}$ and $R^{-1/3}$, respectively. Strictly speaking it is only the first kind that merits the name — double tearing mode — because it straddles the two flux surfaces that are close enough. The second kind is just a combination of two regular standard tearing mode stationed at each of the well-separated rational surfaces. In the double tearing mode the perturbations centered at each rational surface interact with, and enhance each other causing a marked increase in the growth rate. For the regular tearing case, the two rational surfaces are wide apart, and the perturbations centered at each rational surface do not interact but merely develop independently. The structures of the modes are also significantly different. In the double tearing case, the perturbed magnetic flux changes significantly across the tearing layers while it is essentially a constant in the regular tearing case. The perturbed parallel current and poloidal velocity both are nonzero over the whole region between the two rational surfaces and extend far beyond in the former case. Whereas, they peak at the two rational surfaces and are rather localized in the late case. The transition from one to the other occurs at

$$\frac{x_s}{a}|_{\text{crit}} \sim (k_y a)^{-11/15} R^{-1/15}.$$

The small R exponent $1/15 \simeq 0.067$ means that the current profile and the poloidal mode number $k_y = m/r_{\min}$ determine the critical value of x_s. We have also demonstrated that the growth time of the double tearing mode is comparable with current penetration time over the tearing layer. In contrast, the growth time is longer than the current penetration time for the regular tearing mode.

Recently, Mahajan and Yoshida have shown that in a collisionless two-fluid model, a combination of the Hall term and the fluid nonlinearity can lead to the formation of a self-organized singular layer that displays the essential observational features of the thin shear layer associated with the high-confinement (H-mode) tokamak discharges.[19] One of the necessary conditions for the formation of such a layer is a poloidal velocity of the order of poloidal Mach number unity. A similar situation, i.e, the existence of a narrow layer with a strongly sheared flow, exists for tokamak discharges with internal transport barriers (ITB). The mechanisms for the creation of such flows is far from understood. An important clue

does come from the experimental observations that the ITB's are often formed around low mode number rational surfaces (Ref. 20 and the references therein). Coupled with the fact that the magnetic energy released in the reconnection process following the development of a tearing mode can drive large flows, we are tempted to suggest that the tearing mode studied in this work may provide a possible trigger for the formation of the singular layers or ITBs. We do not attempt to describe the detailed dynamics here but make a rough nonlinear estimate for the amplitude of the saturated poloidal velocity.

Balancing shearing frequency in the first and viscous dissipation rate in the third term on the right-hand side of Eq. (6), we find

$$k_y V_y \sim \frac{k_\perp^4 \mu_e c^2}{\omega_{pe}^2} = v_A \frac{k_\perp^4 a^4}{R\alpha}.$$

where v_A is the poloidal Alfvén velocity and $k_\perp^2 = k_x^2 + k_y^2 \simeq k_x^2$. With

$$k_x \sim \Delta^{-1} \simeq (\lambda\sigma)^{-1/6} \simeq \left[\gamma\tau_h/(\alpha B'_{0y})^2 R\right]^{-1/6},$$

and

$$\gamma\tau_h \sim \lambda \sim R^{-1/5},$$

it is easy to estimate that the saturated poloidal shearing velocity compared with the thermal velocity is

$$\frac{V_y}{v_T} \sim R^{-1/5}.$$

For $R \sim 10^5$, this is the just the magnitude required (Ref. 19) for strong sheared flows in the layer. It is worthwhile to point out that the resistivity driven double tearing modes will generate similar levels of saturated poloidal flows for rather low $S \sim 10^3$ making them unlikely to be the sources for ITB creation. The viscosity driven double tearing mode, on the other hand, seems eminently suited for the job.

We have not dwelt much on the underlying physical mechanisms that may lead to the anomalous electron viscosity. The braiding magnetic field lines (Ref. 16) created by higher mode number MHD instabilities is one possible mechanism. Another possible source could be the unstable electromagnetic micro-modes characteristic to high β(= plasma pressure/magnetic pressure) plasmas.[21,22] Since the double tearing modes driven by the electron viscosity may play an important role in the processes of flow creation, it would be worth our while to thoroughly examine and investigate the origin of anomalous μ_e.

Acknowledgments

This work is supported by the Associateship of The Abdus Salam International Center for Theoretical Physics, Trieste, Italy, by the National Natural Science Foundation of China, Grant No. 10075015 and by U.S. Department of Energy, Grant No. DE-FG03-96ER-54346.

References

1. L.L. Lao, K.H. Burrell, T.S. Casper, V.S. Chan, S.M. Chun *et al.*, Phys. Plasmas **3**, 1951 (1996).

2. Y. Koide, M. Kikuchi, M. Mori, S. Tsuji, S. Ishida *et al.*, Phys. Rev. Lett. **72**, 3662 (1994).

3. P. L. Pritchett, Y. C. Lee, and J. F. Drake, Phys. Fluids **23**, 1368 (1980).

4. S.M. Mahajan, R.D. Hazeltine, Nucl. Fusion **22**, 1191 (1982).

5. D. H. J. Goodall and J. A. Wesson, Plasma Phys. Controlled Fusion **26**, 789 (1984).

6. J. W. Connor, S. C. Cowley, R. J. Hastie, T. C. Hender, A. Hood, and T. J. Martin, Phys. Fluids **31**, 577 (1988).

7. R. G. Kleva, J. F. Drake, and R. E. Denton, Comments Plasma Phys. Controlled Fusion **13**, 63 (1989).

8. L. Ofman, Phys. Fluids B **4**, 2751 (1992).

9. R. L. Dewar and M. Persson, Phys. Plasmas **1**, 1256 (1994).

10. Qingquan Yu, Phys. Plasmas **3**, 2898 (1996).

11. B. B. Kadomtsev, *Tokamak Plasma: A Complex Physical System* (Institute of Physics, Bristol, 1992).

12. S. D. Scott *et al.*, Plasma Physics and Controlled Nuclear Fusion (International Atomic Energy Agency, Vienna, 1989), Vol. 1, P. 655.

13. S. V. Konovalov, A. B. Mikhailovskii, M. S. Shinokov, and V. S. Tsypin, Phys. Plasmas **9**, 4596 (2002).

14. M.N. Rosenbluth, P. H. Rutherford, in *Fusion*, edited by E. Teller, (Academic Press, New York, 1981), vol. 1, Part A, p. 31.

15. P. K. Kaw, E. J. Valeo, and P. H. Rutherford, Phys. Rev. Lett. **43**, 1398 (1979).

16. A.Y. Aydemir, Phys. Fluids B **2**, 2135, (1990).

17. B. Coppi, R. Galvao, R. Pellat, M. N. Rosenbluth, and P. H. Rutherford, Fiz. Plaszmy **2**, 961 (1976) [Sov. J. Plasma Phys. **2**, 533 (1976)].

18. F. Oberhettinger, in *Handbook of Mathematical Functions*, edited by M. Abramowitz and I. A. Stegun (Dover, New York, 1968), p. 555.

19. S.M. Mahajan and Z. Yoshida, Phys. Plasmas **7**, 635 (2000).

20. E. Joffrin C.D. Challis, G.D. Conway *et al.*, Internal Transport Barrier triggering by rational flux surfaces in tokamaks, IAEA 19th Fusion Energy Conference, Lyon, France (October, 2002). Submitted to Nucl. Fusion.

21. J. Q. Dong, L. Chen, and F. Zonca, Nucl. Fusion **39**, 1041 (1999).

22. Z. Gao, J. Q. Dong, G. J. Liu, and C. T. Ying, Phys. Plasmas **8**, 4080 (2001).

Figure Captions

1. Dispersion relation $\widehat{\lambda}$ versus $\widehat{\lambda}_h$ [Eq. (45)].

2. Normalized growth rate $\gamma\tau_h$ as a function of the wavenumber α for $x_s = 0.25$ (a) and 0.7 (b).

3. Normalized growth rate as a function of the fluid dynamic Reynolds number R for $x_s = 0.25$ (the short line) and 0.7 (the longer line).

4. Perturbation of the magnetic flux ψ_1 and the displacement, ξ (a), and the perturbation of the parallel current density j_{1z} and the poloidal velocity V_y (b) as functions of x for $x_s = 0.25$.

5. The same as Fig. 4 but for $x_s = 0.7$.

6. The same as Fig. 4 but for $x_s = 0.1$.

Dong *Fig. 1*

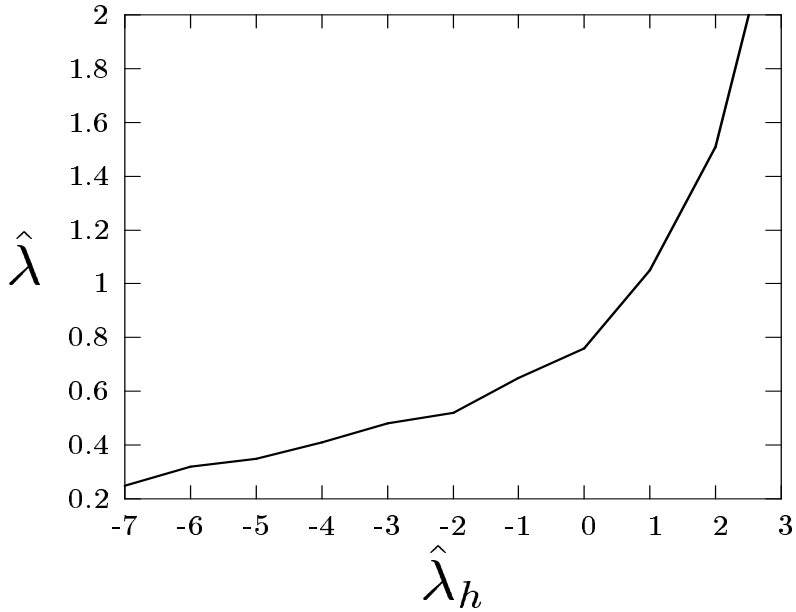

Dong *Fig. 2*

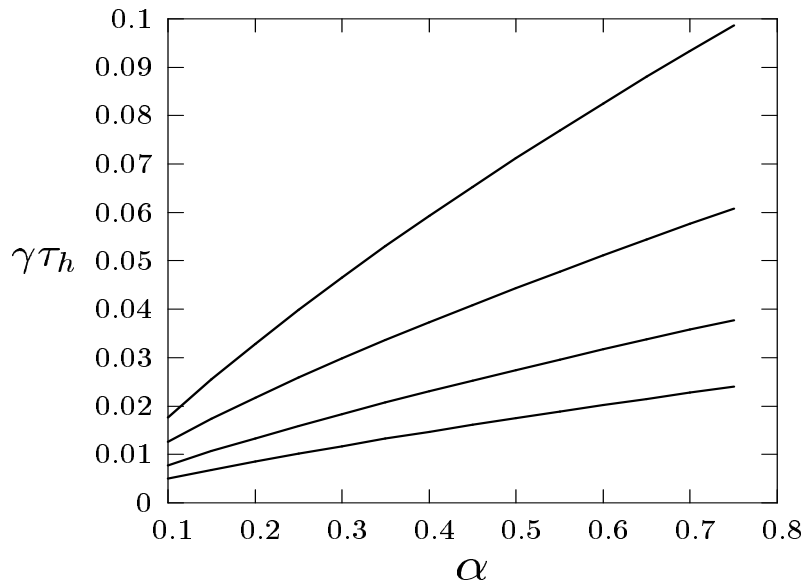
0.1
0.09
0.08
0.07
0.06
$\gamma\tau_h$ 0.05
0.04
0.03
0.02
0.01
0
0.1 0.2 0.3 0.4 0.5 0.6 0.7 0.8
α

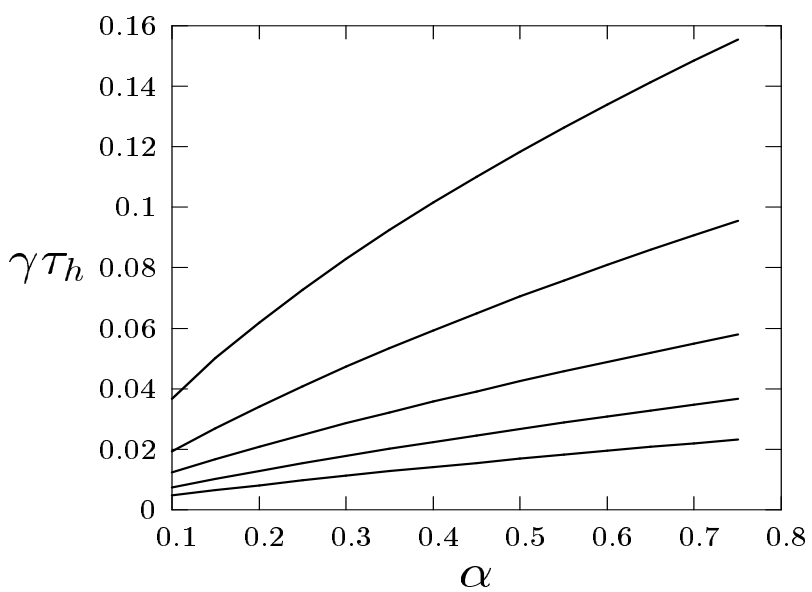
0.16
0.14
0.12
0.1
$\gamma\tau_h$ 0.08
0.06
0.04
0.02
0
0.1 0.2 0.3 0.4 0.5 0.6 0.7 0.8
α

Dong *Fig. 3*

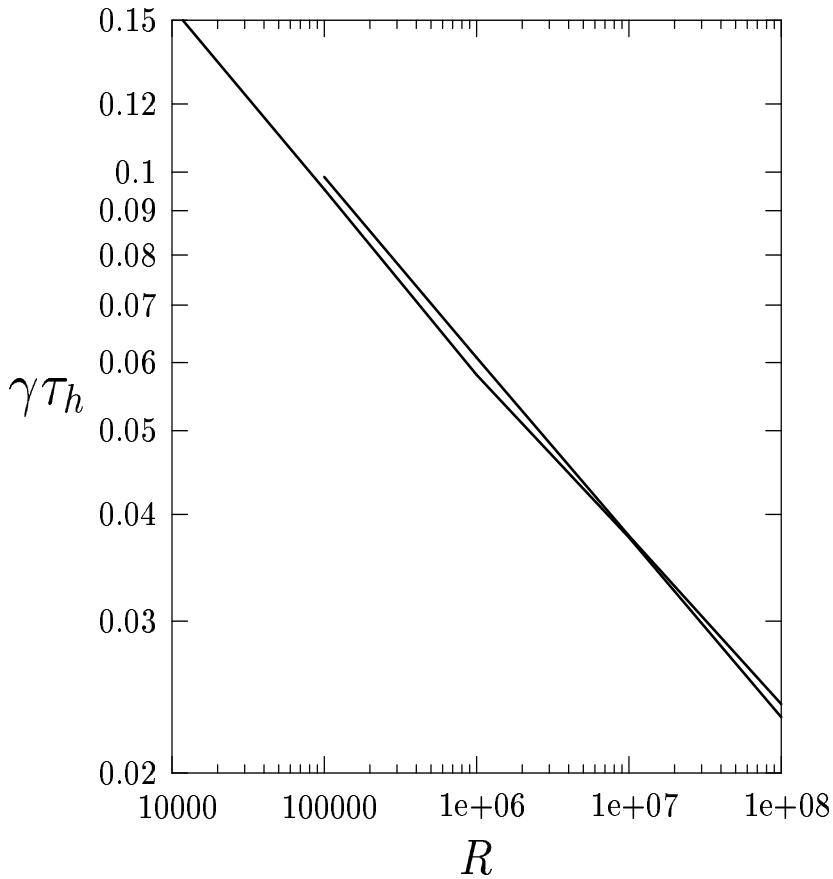
0.15
0.12
0.1
0.09
0.08
0.07
0.06
0.05
0.04
0.03
0.02
$\gamma\tau_h$
10000
100000
1e+06
1e+07
1e+08
R

Dong *Fig. 4*

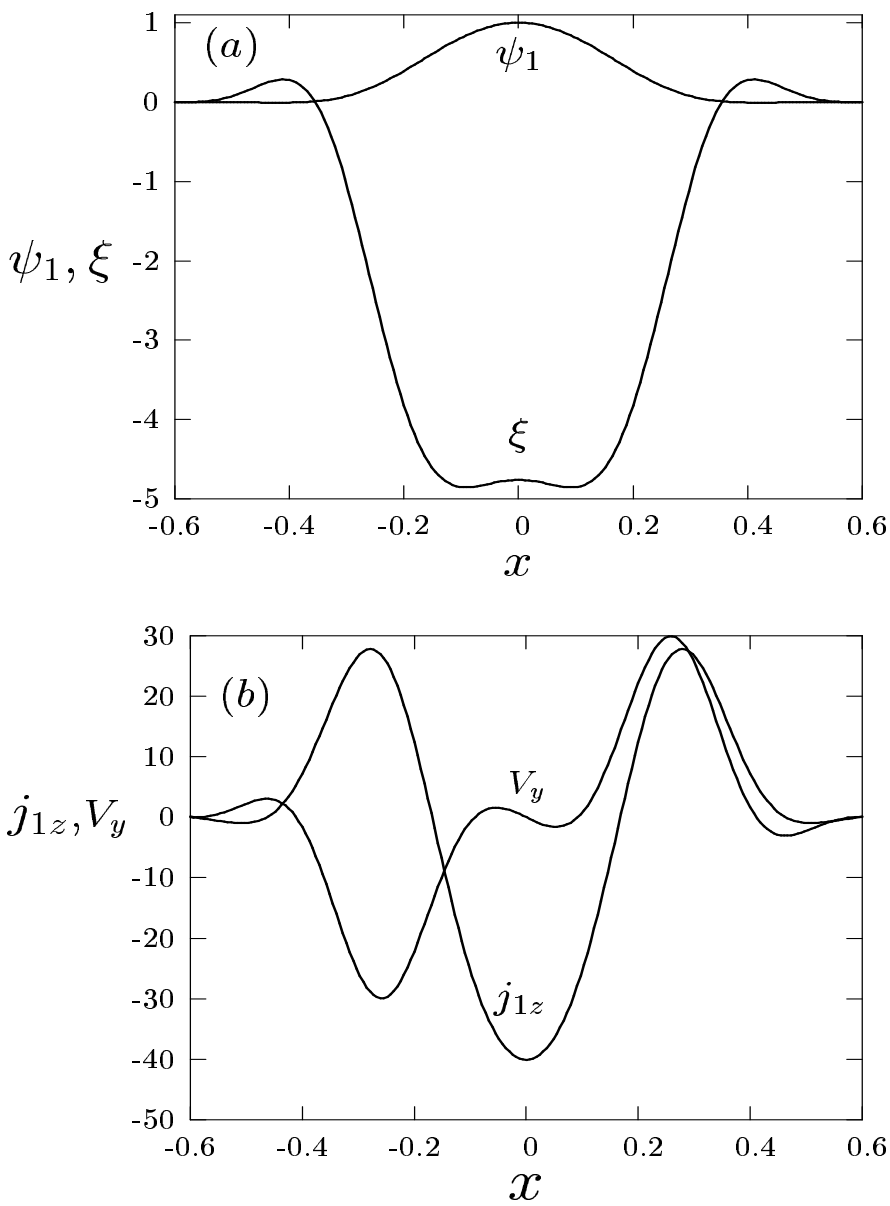
(a)
ψ_1
ξ
ψ_1, ξ
1
0
-1
-2
-3
-4
-5
-0.6
-0.4
-0.2
0
0.2
0.4
0.6
x
(b)
V_y
j_{1z}
j_{1z}, V_y
30
20
10
0
-10
-20
-30
-40
-50
-0.6
-0.4
-0.2
0
0.2
0.4
0.6
x

Dong *Fig. 5*

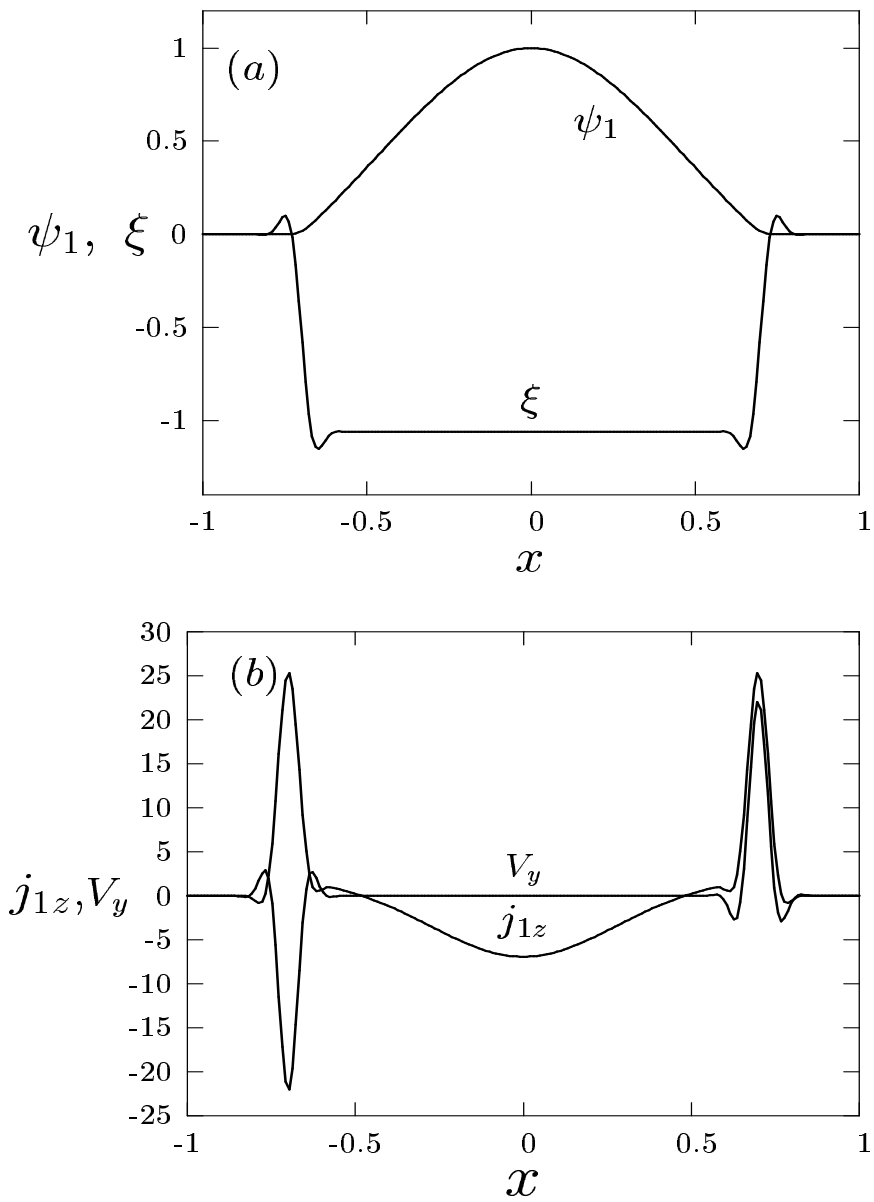
(a)
ψ_1
ξ
$\psi_1,\ \xi$
1
0.5
0
-0.5
-1
-1
-0.5
0
0.5
1
x
(b)
V_y
j_{1z}
j_{1z}, V_y
30
25
20
15
10
5
0
-5
-10
-15
-20
-25
-1
-0.5
0
0.5
1
x

Dong *Fig. 6*

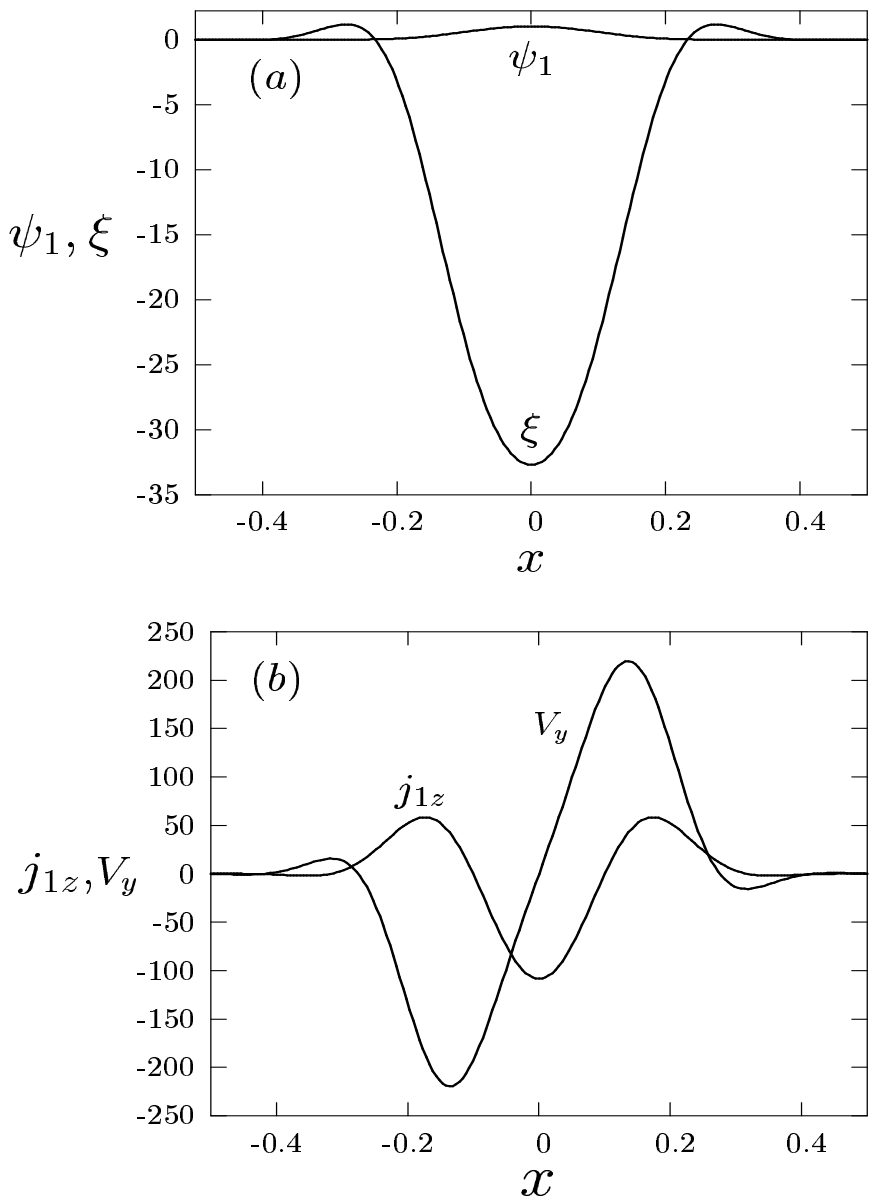
(a)
ψ_1
ξ
ψ_1, ξ
0
-5
-10
-15
-20
-25
-30
-35
-0.4
-0.2
0
0.2
0.4
x
(b)
V_y
j_{1z}
j_{1z}, V_y
250
200
150
100
50
0
-50
-100
-150
-200
-250
-0.4
-0.2
0
0.2
0.4
x